

# D5.1 EISCAT\_3D Radar Imaging Arrays Configurations Report

Tom Grydeland and César La Hoz

September 2006

## **Abstract**

The adopted two-level architecture for antenna beam forming is an optimum global solution that also satisfies the requirements of interferometric imaging, as the module antennas of the second level constitute the antenna units upon which antenna baselines can be constructed with great flexibility. On the basis of this architecture, some advantageous geometric patterns into which the module antennas can be organized into baselines are described for various sizes and geometries of the main array.

The tasks on the real-time processing which fall under work package 5: interferometry, are outlined: namely, that a few baselines in orthogonal directions be monitored to detect interesting events to be saved for imaging. Different possibilities for conditions and decision-taking are described including criteria for the selection of type of parameter to monitor and possible threshold values.

# 1 Background

## 1.1 Antennas, elements, modules, arrays

For the purpose of this document, the individual crossed dipoles are called *elements*, or *element antennas*, a local collection of antennas is called a *module*, and all modules are placed in an *array* to constitute the complete radar antenna. Most modules will comprise active (i.e. transmit/receive) elements and be localised within a roughly circular aperture. We will refer to the array constituted by these modules as the *core* antenna, or core array. For interferometry, a small number of modules will also be constructed outside the core. We will refer to these as *outlier modules*.

The term *module* is used in the same way as for the Jicamarca array, and corresponds to the term *station* in the LOFAR organisation. The term *core* is used in a similar way as for LOFAR. Our *module beams* (defined below) correspond to the *station beams* of LOFAR.

## 1.2 Beam forming architecture

Regardless of the choice of architecture, digital beam forming would be a significant part of the receiver system, both for ordinary (full-array beams) and interferometric (module beams) modes of operation for the EISCAT\_3D system.

For digital beam forming, the digital signal from each antenna element is subjected to a combination of delay and phase shifts (and possibly attenuation), DP/A, depending on its position within the array and the desired beam direction and shape. The signals from all elements are then combined (added) to form a single beam. On the receive side, multiple DP/A functions can be applied to independent copies of the element signals to form multiple independent beams. For interferometry, beam forming must be done at the level of modules (local groups of elements), while for ordinary radar operations, the full array is used for beam forming. Since addition is associative, it is obvious that beams formed in modules for interferometry can also be considered intermediate or partial sums in the beam forming for the full array.

During preparatory discussions leading up to the meeting between WPs 4, 5, 8 and 9 in Kiruna in early July, it became clear that significant savings in complexity and reuse of effort could be achieved if the architecture for digital beam forming could be modified, leading, at the same time, to a nearly optimum architecture for interferometry, as the modified scheme allows for

greater flexibility to configure the array for different interferometric applications at the level of conventional programming/data-processing. At the same time, the complex task of data distribution in the general purpose beam forming process is broken down into much simpler local data distribution tasks in a “divide and conquer” strategy. The discussion has been summarised by McKay [5]. On the basis of these ideas, during the meeting in Kiruna, the suggested two-level beam forming architecture was refined and agreed upon [4]. The modified architecture is simpler to implement and produces identical results for the full array beams, while it eliminates the need for separate beam formers for interferometry, increases the configuration flexibility considerably, and it immediately provides interferometric capability for all receive beams. The architecture is illustrated in figure 1.

The combination of signals into beams will happen in two stages. In the first stage, *module beam formers* (BF in the diagram) will apply DP/A and sum signals from groups of approximately 600 elements into *module beams*, and the module beams from all modules (starting from about 20, but growing over time) are simply added to form the full beam in the second stage.

At the same time, module beam signals are also routed to *interferometric receivers* (IRX in the diagram) where they are downsampled to a bandwidth matched to ion line observations. The module beam signals are then the starting points for interferometric signal processing.

An important consequence of the two-level beam forming architecture for the design tasks is that it eliminates the need for fixed or hardwired antenna configurations for interferometry. Thus, this aspect of the design task will investigate optimum or near optimum antenna configurations for different interferometric applications which can be implemented in software, very possibly at the experiment design level. The configurations that can be obtained are limited only by the chosen size of the “modules” in the first level and by the longest linear dimension of the entire array. An important task of the design process is then to survey the parameters of the limiting configurations. In a way, these parameters will represent the formal specifications of the EISCAT\_3D imaging interferometer.

## 2 Interferometric signal processing

Data for interferometry will be stored as amplitude data, for a number of reasons:

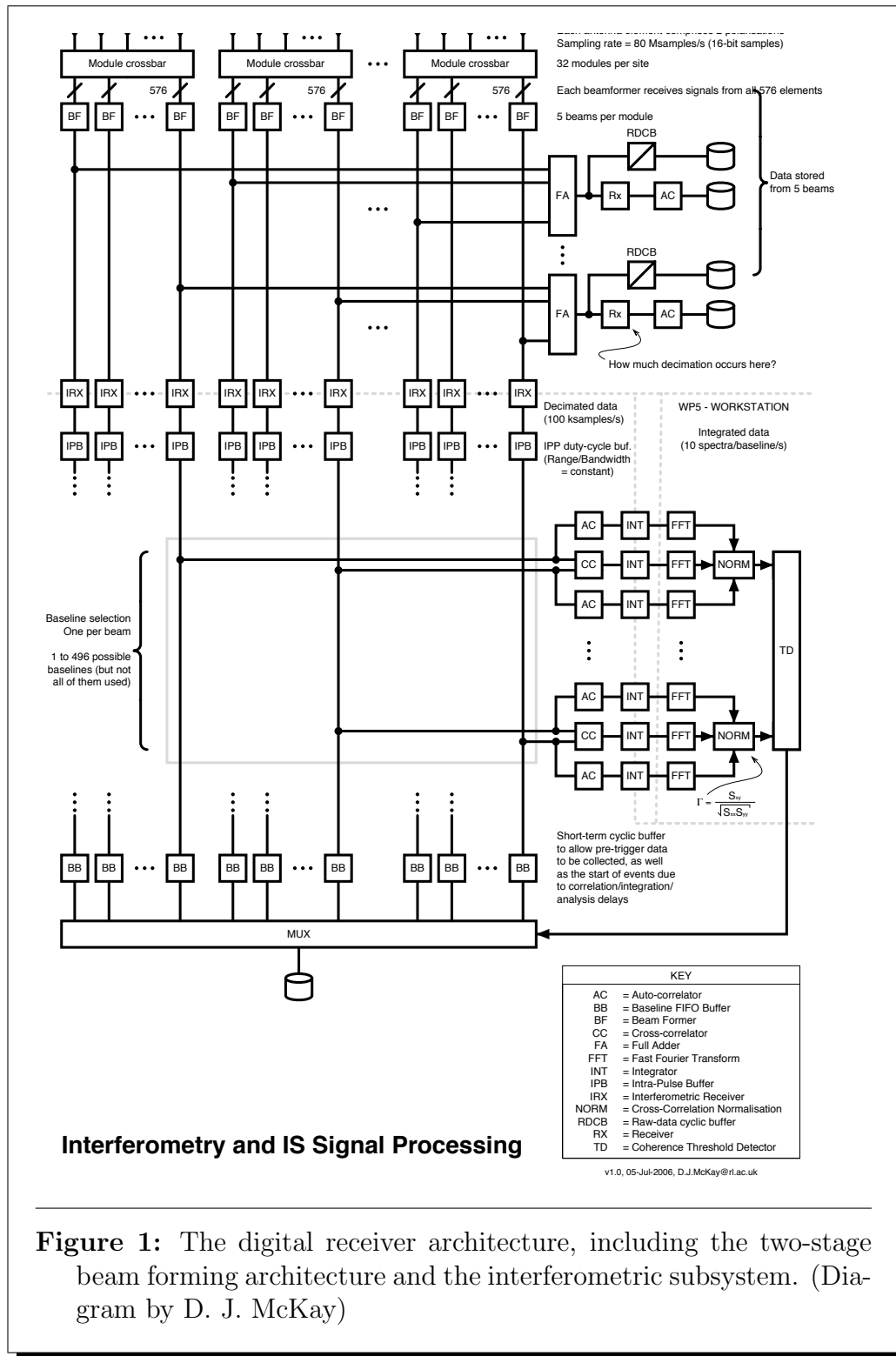


**Figure 1:** The digital receiver architecture, including the two-stage beam forming architecture and the interferometric subsystem. (Diagram by D. J. McKay)

- at time resolution of 0.1 s, the amount of cross-correlated and auto-correlated module data at each baseline is significantly larger than the amplitude data from a pair of channels.
- the number of baselines increases quadratically with the number of modules used for interferometry
- amplitude data gives greater flexibility for off-line re-processing

The purpose of the real-time processing is then to decide when to store amplitude data from the interferometry subsystem. The production of images from the amplitude data that is stored will be made off-line.

For this purpose, it is sufficient to monitor a small number of non-parallel baselines. Which baselines to monitor is discussed in the next section.

For every baseline which is to be used for the real-time decision, it is necessary to compute the profile of cross-correlation functions between the two modules involved and, for normalisation purposes, the profiles of auto-correlation functions in each module. Each of these profiles is then used to produce a spectrum profile by means of a discrete Fourier Transform (DFT). The decision process can then consider correlation functions, coherences and their phases when making the decision.

As agreed upon in Kiruna, the computation of correlation function profiles is best done in a dedicated real-time system, which may share significant characteristics with the processing units used for the full beam incoherent scatter processing. The decision process on the other hand is likely to undergo development as experience is gained and will only consider data integrated to the 0.1 s resolution, so it is probably preferable and quite feasible to implement this in one or a small number of ordinary workstations.

The way integrated and correlated data enters this workstation from WP9 (signal processing) hardware needs to be defined. Similarly, the way a “store” message is to be created and transmitted to the WP8 (archiving) system must be defined.

## 2.1 Parameters characterizing the real-time interferometric signal processing

Although the number of baselines for the real-time interferometric system will be quite small, they require the processing of a number of profiles probably exceeding that of the regular signal processing chain. On the other hand, these will be computed at the reduced bandwidth and sampling rate of the interferometric subsystem, so this resulting computational burden is likely

to be no higher than that in the ordinary system for a given range and lag coverage.

As there is no interferometric data available which has previously been gathered with similar arrays at these frequencies, it is not known what the properties of targets of interest are going to be. Spectral characteristics and occurrence frequencies can be expected to be similar to what has been observed at EISCAT VHF. Signal to noise ratios should be better than what has been seen in the EASI array on Svalbard (due to both the lower frequency and the larger size of the modules of EISCAT.3D), but a good deal worse than that seen in ordinary incoherent scatter radars.

In the interferometric results obtained with the interferometric technique at the EISCAT Svalbard Radar, the cross-spectrum has at times shown as much spectral information as the power spectra in each of the two antennas. Strong echoes with meaningful coherence have also been seen at all ranges from below 150 km up to more than 800 km.

The recommendation is therefore to process all ranges and lags allowed for by the transmitted modulation (out to at least where the third zero crossing occurs for incoherent scattering) and the entire receive interval. If experience shows that the selection in practice does not require all these lags and ranges, the processing parameters can be relaxed.

## 2.2 Potential selection criteria

By a reasoning like that above, the selection criteria used should probably be set with quite low thresholds to begin with, to allow for false positives (data stored without interesting features) and minimise the number of false negatives (interesting features lost).

Furthermore, the buffers on interferometric data should be used such that recordings start 1/2 to 1 second before a criterion was triggered, and to continue for as long after a trigger. The records should also incorporate what selection criteria were triggered, and at what ranges.

### 2.2.1 Coherence

Since coherence is the computed quantity which is directly linked to the size of a scattering structure, the most obvious selection criterion is some sort of threshold for coherence. A relatively advanced technique such as Hildebrand and Sekhon [2] should be used to estimate the noise level in the coherence profile. The technique establishes the highest possible threshold where

everything below the threshold behaves statistically as white noise. Therefore, everything above the threshold is coloured, and should be considered for selection.

Thresholding on coherence alone is not without its troubles, however. At 0.1 s integrations, even the 32 m and 42 m antennas of the ESR do not produce very high signal levels. Hence, through the normalisation used to compute coherence, high levels will sporadically occur in integration intervals and range/frequency regions where there are no targets of interest. It may be necessary to also consider the phase behaviour in the region of high coherence.

### 2.2.2 Cross-correlation levels

From the ESR data, another possible criterion seems possible — selection on the relative strength of cross-correlation and auto-correlations. From the profiles of the auto-correlations, the maximum of the real part (i.e. the zero lag) is taken at every range and the geometric average between the signals in the two modules is computed. This is compared to the maximum of the absolute value of the cross-correlation between the signals (which is not necessarily at zero lag).

The selection criterion in this case is that the cross-correlation exceeds a certain fraction of the average auto-correlation. The actual fraction must again be determined by experience, but in the ESR data from the 32 m and 42 m antennas seems to suggest that a useful threshold will be around 25 %.

### 2.2.3 Abrupt signal level changes

One of the features often seen in plasma turbulence events is abrupt appearance and disappearance of enhanced scattering. Another useful selection criterion might be to see when the signal level changes by large amounts or large fractions from one 0.1 s period to the next. Such abrupt changes might also be of interest in the absence of interferometric targets.

## 2.3 Satellite echoes and interferometry

Echoes from artificial satellites share many of the characteristics of the echoes we want to catch with the interferometric technique. In the absence of effective satellite suppression techniques (e.g. static or adaptive null forming on the transmit and/or receive beams) we should expect several satellites to be selected by these criteria.

Initially this can be considered beneficial, since it will provide us with an abundance of strong, localised targets with which to test and evaluate our detection and imaging algorithms. Comparison between satellite positions given by interferometric and other means (e.g. ephemeris data or optical observations) will also be useful input to the phase calibration process.

### 3 Antenna configurations for interferometry

The task of designing a configuration of modules suitable for interferometry is considered in two stages: a configuration for the core (involving a subset of the core modules), and the configuration of outlier antennas. For the core itself, we discuss the possibility of randomly placed modules, as well as optimally selected subsets of various regular (dense) core arrangements.

For random configurations, simulations have been carried out. In these cases, the centre positions of modules were drawn from some distribution (described below for each case). The resulting baseline pattern was then computed, and Fourier transformed to produce the synthesised beam. Configurations were then evaluated by the highest sidelobe level seen in the synthesised beam inside a field of view slightly larger than the transmit beam, or about  $2^\circ$  in diameter. The configuration with the smallest maximum sidelobe inside this field of view was selected.

#### 3.1 Configuration for the core

The typical way of building an array from a number of element antennas is to arrange them in a regular grid. This has significant engineering and organisational advantages, but it does not produce the cleanest possible beam. Every pair of antennas produces an interference pattern, and when elements are placed in a regular grid, exaggerated sidelobes are produced as all of these pairwise patterns interfere constructively in regions outside the intended beam. A more randomised antenna distribution results in a sidelobe pattern with less regularity and where the energy in the sidelobes is distributed more evenly.

The architectural division of the core array into modules for signal processing purposes also allows for a partially randomised array by randomizing the position of the modules that constitute the core. A narrower beam results when the modules are spaced out, at the cost of more energy in the sidelobes. Randomizing the spacing of the modules means that the sidelobes are kept at a lower and more uniform level, even with the narrower main beam. The

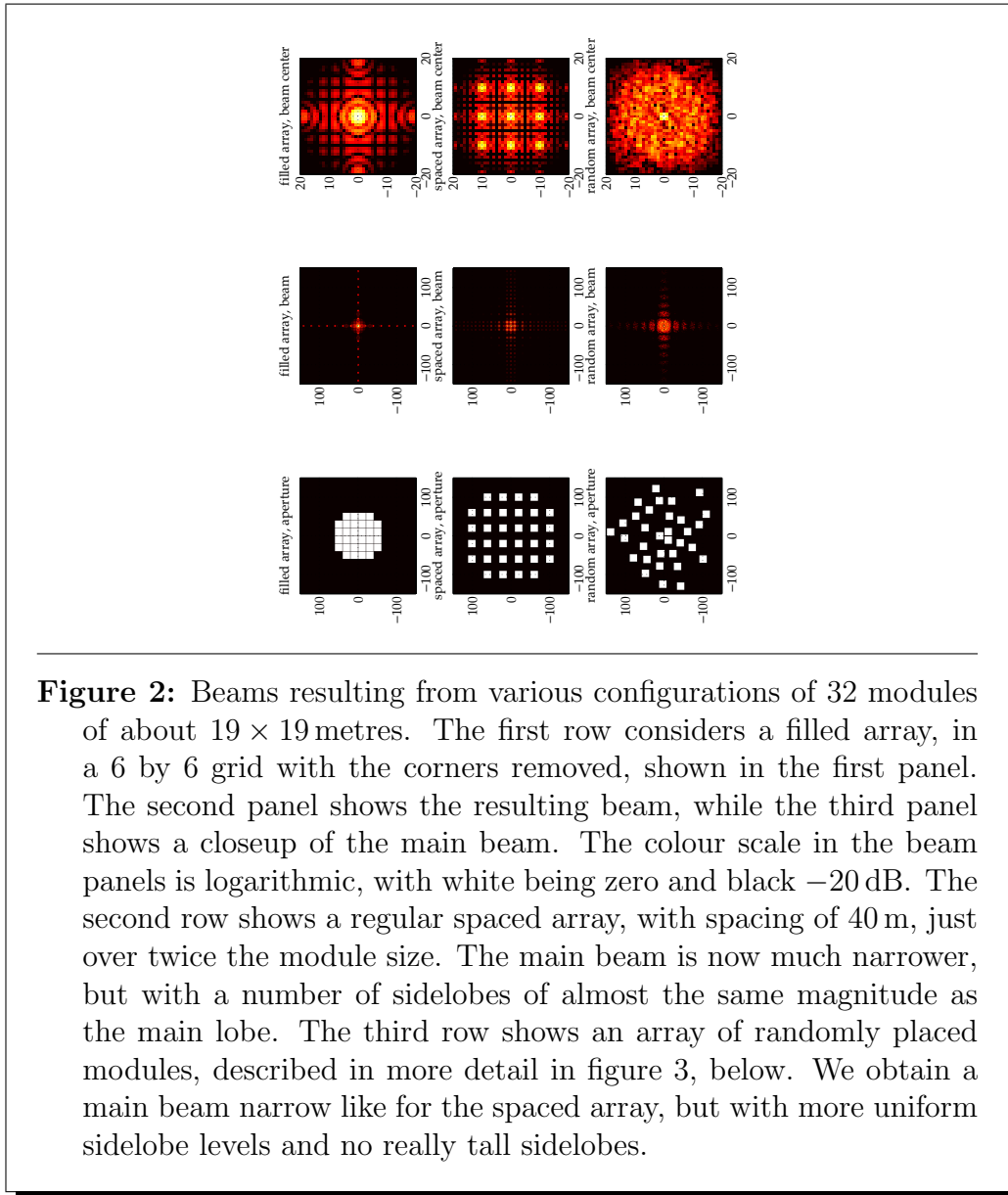
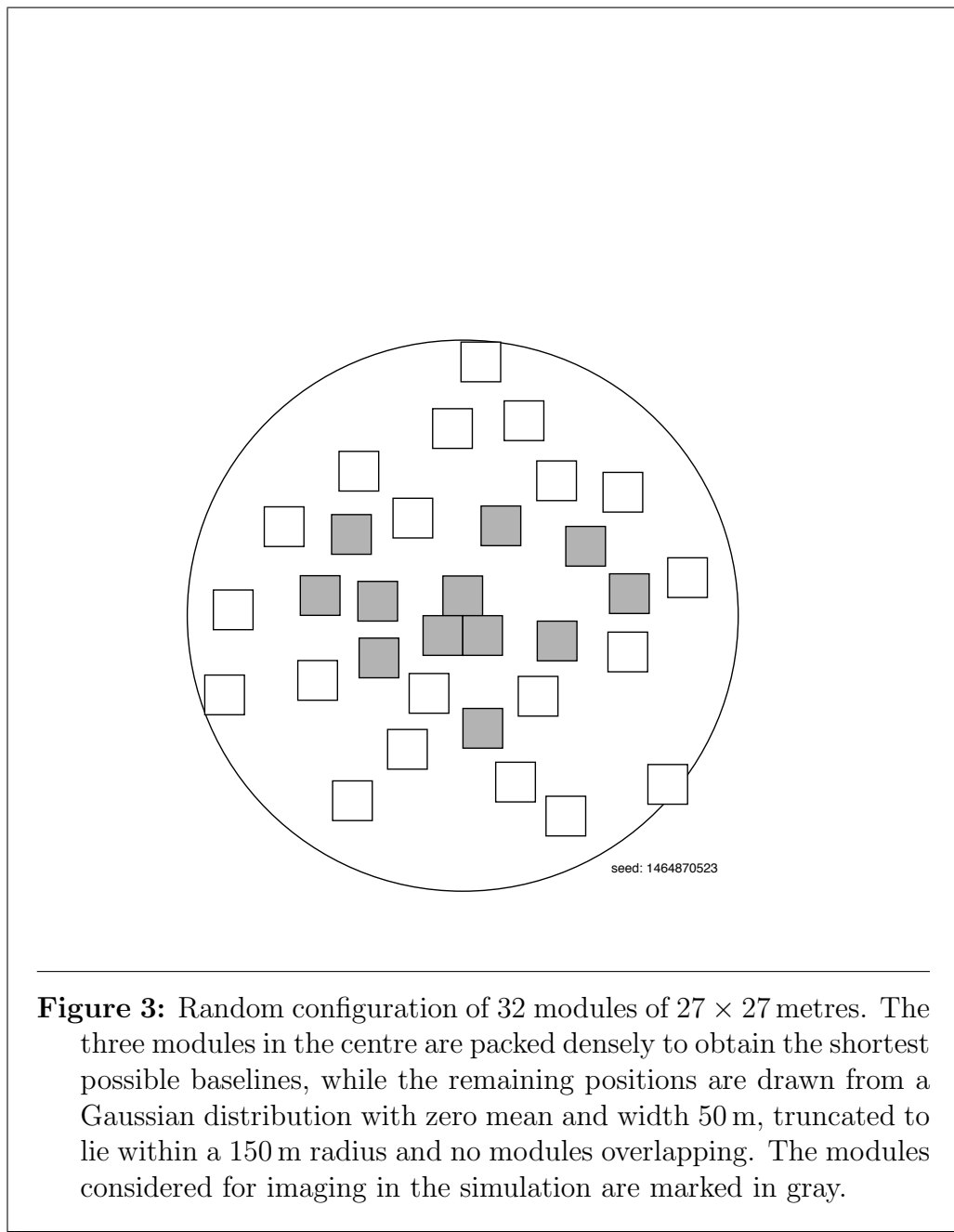


**Figure 2:** Beams resulting from various configurations of 32 modules of about  $19 \times 19$  metres. The first row considers a filled array, in a 6 by 6 grid with the corners removed, shown in the first panel. The second panel shows the resulting beam, while the third panel shows a closeup of the main beam. The colour scale in the beam panels is logarithmic, with white being zero and black  $-20$  dB. The second row shows a regular spaced array, with spacing of 40 m, just over twice the module size. The main beam is now much narrower, but with a number of sidelobes of almost the same magnitude as the main lobe. The third row shows an array of randomly placed modules, described in more detail in figure 3, below. We obtain a main beam narrow like for the spaced array, but with more uniform sidelobe levels and no really tall sidelobes.

organisational and engineering benefits of the regular array are still reaped by having each module be highly structured and identical. The beams produced by using a dense array, a sparse and regular array, and a random array are presented and compared in figure 2.



### 3.1.1 Random core configuration

For interferometry, it is desirable to have baselines which are not multiples, linear combinations or rotations of each other, something randomised modules will help achieve. As an example of what such a configuration would look

like, we performed a search as explained above. Modules of  $21.6 \times 21.6$  m were considered in this simulation. Three modules were placed, densely packed in the centre of the array to provide as short baselines as possible, while the rest of the module positions were drawn from a Gaussian distribution with zero mean and width 50 m, and module positions draws which would overlap with already placed modules, or at a distance of more than 150 m from the centre of the array were discarded. A total of 32 modules were placed, and the first 12 modules were used to test the usefulness for interferometry. Figure 3 shows the best configuration arrived at during this search. The modules marked in gray were the ones used in the testing.

### 3.1.2 Selection of modules in a filled core array

In the case of a regular, filled array, the module positions are given by the grid, and when selecting from which modules data should be stored for interferometry, the object must be to achieve as complete as possible a coverage of all the baselines which can in theory be achieved from the array. In practice, we have found that there is a most obvious number of modules for an array of a given size. Using fewer modules means leaving great gaps in the baseline diagram, while having more modules does not add a great deal. The two-level beam forming architecture gives great flexibility regarding exactly which baselines to monitor for interferometric events, so there is no reason to think that other patterns of modules cannot also be used. We have considered a few possible configurations of regular modules which result in a roughly circular aperture of about 80 m in diameter, and also the same kinds of configurations with the number of elements per module as  $24 \times 24$  for square modules, or 547 elements in 27 rows for hexagonal modules.

In figure 4, a configuration using 21 square modules arranged in a five by five grid with the corner modules missing is shown. For interferometry, 8 modules out of the total 21 are used. With the configuration shown in the left part of the figure, most of the baselines possible from such an array can be obtained, with very few redundant baselines. Expanding to 9 modules increases the number of baselines achieved from 26 to 30, which appears to be past the point of diminishing returns.

For an array of about 80 m in diameter, the modules should be about 16 m square. At 240 MHz and with an element spacing of  $0.9 \lambda$ , this means modules of  $14 \times 14$  elements. If, on the other hand, the modules are  $24 \times 24$  elements, or 27 m square, the array comes to a diameter of 135 m. The total number of elements in these two cases is 4116 and 12096, respectively.

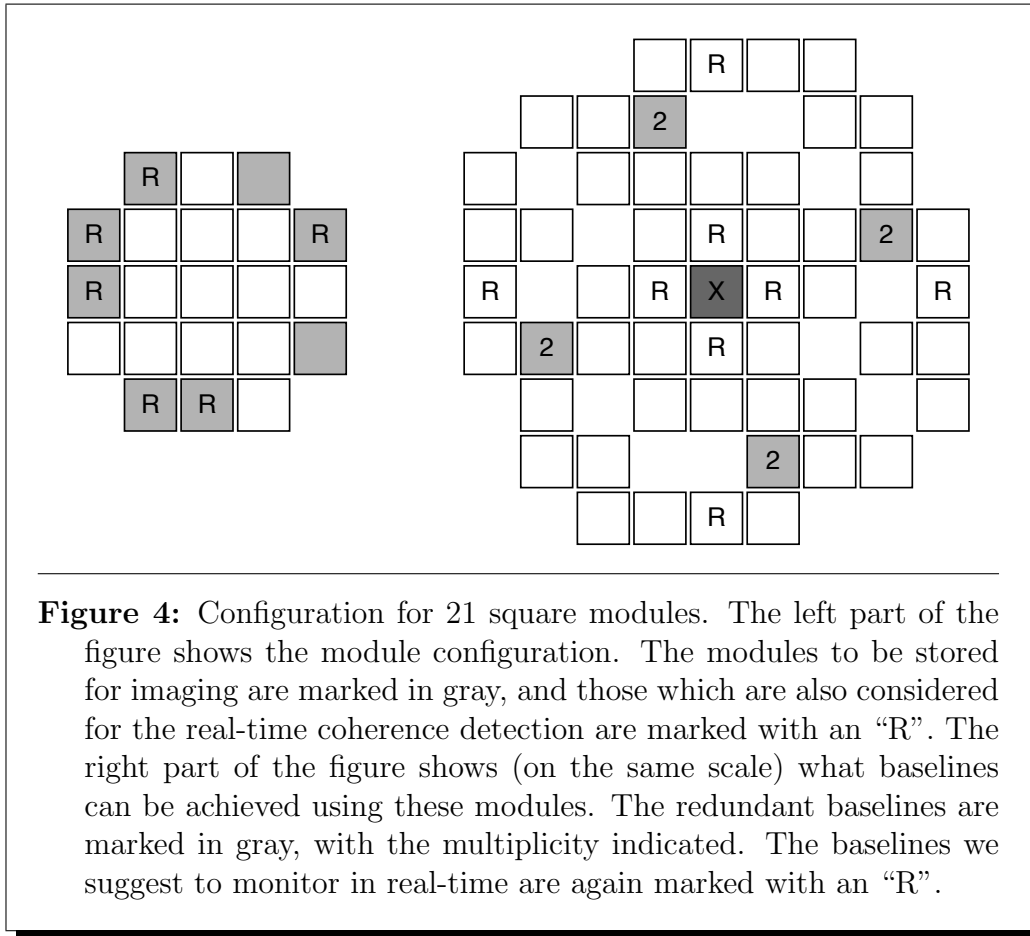
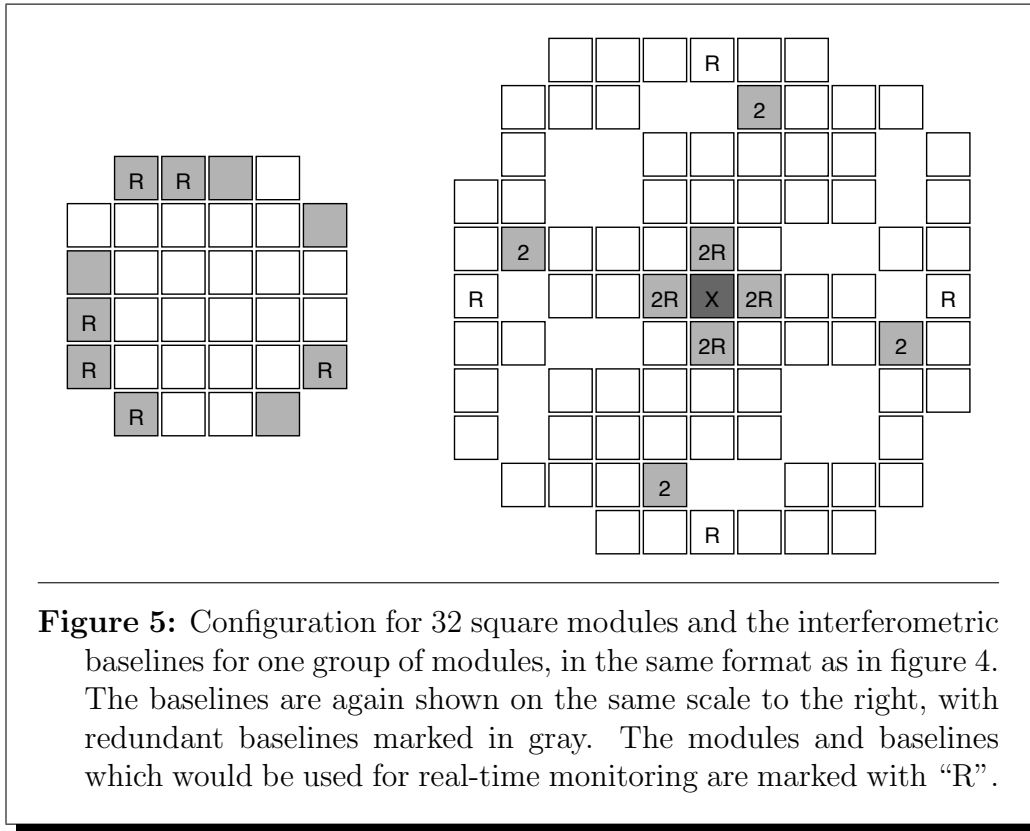


**Figure 4:** Configuration for 21 square modules. The left part of the figure shows the module configuration. The modules to be stored for imaging are marked in gray, and those which are also considered for the real-time coherence detection are marked with an “R”. The right part of the figure shows (on the same scale) what baselines can be achieved using these modules. The redundant baselines are marked in gray, with the multiplicity indicated. The baselines we suggest to monitor in real-time are again marked with an “R”.

With this configuration, a total of 26 distinct baselines, shown in the right part of the figure, are achieved, of a theoretical maximum (for 8 modules) of 28, while the total number of possible baselines within this array is 34. For modules of 16 m square (27 m square), baselines range from 12.6 to 50.4  $\lambda$  (21.6 to 86.4  $\lambda$ ).

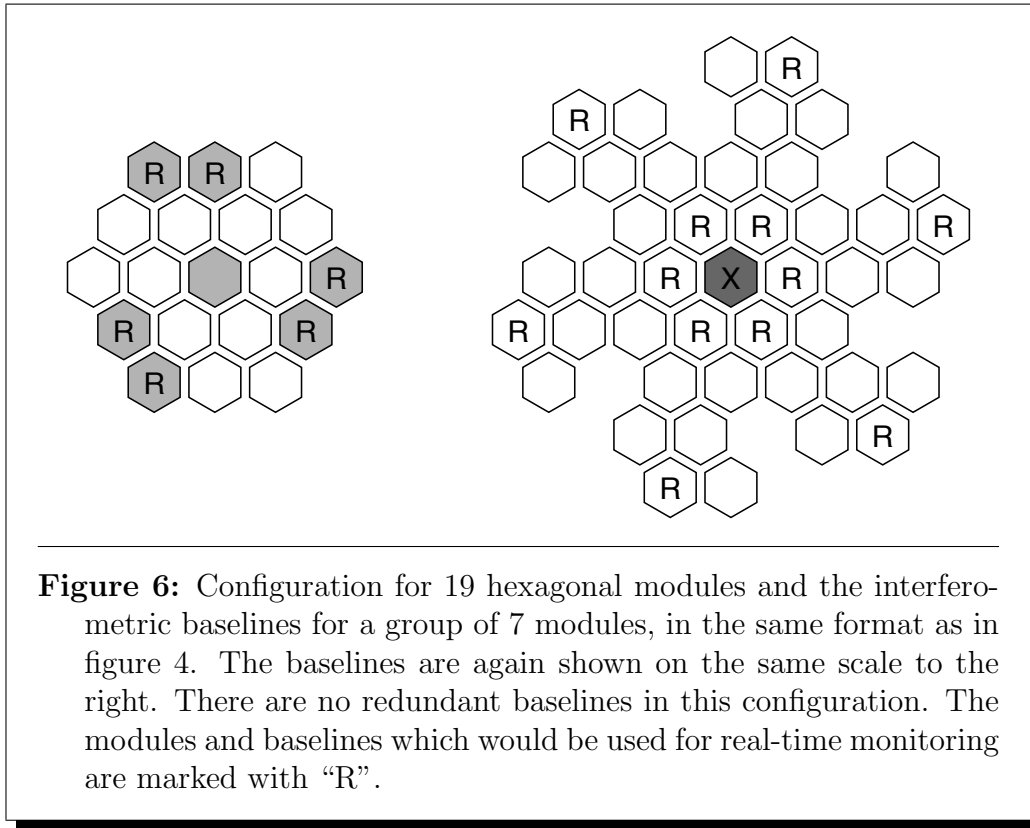
In figure 5, we show a similar configuration, this time for 32 square modules arranged in a six by six grid, again with the corner modules missing. The optimum number of modules to select for interferometry from such an array appears to be 10. With the 10 modules marked in the left part of figure 5, 41 of 56 distinct baselines are obtained, as is shown in the right part of the figure. Using 11 modules achieves a maximum of 45 baselines. For a total diameter of about 80 m, the modules should be  $12 \times 12$  elements, 4608 elements in total. For modules of  $24 \times 24$ , the total number of elements is 18432 and the diameter is 162 m. For modules of  $12^2$  and  $24^2$  elements, the baselines range from 10.8 to 54  $\lambda$  and from 21.6 to 108  $\lambda$ , respectively.



Another possibility for a regular filling of an aperture is to use hexagonal modules. In a hexagonal arrangement, an inter-element spacing of  $0.9\lambda$  means a distance between rows of elements of about  $0.78\lambda$ , or  $0.97\text{ m}$  at  $240\text{ MHz}$ .

In the left part of figure 6, we show a configuration with 19 hexagonal modules in a hexagonal grid of 5 lines. In such a grid, a total of 30 baselines are possible. The figure also shows a very pretty 7-module configuration which provides 21 of these baselines with no redundant baselines. The baseline coverage is shown in the right part of the figure. The modules and baselines to be used for real-time monitoring are marked with an “R” as before. Increasing to 8 modules gives maximum 25 baselines.

For a total array diameter of about  $80\text{ m}$ , each module should comprise 217 elements in 17 rows, for a total of 4123 elements. For modules closer in size to the  $24^2$  discussed earlier, each module should comprise 547 elements in 27 rows, for a diameter of  $135\text{ m}$  and 10393 elements total. For 17-row modules, the baselines range from  $13.25$  to  $46\lambda$ , while 27-row modules give us baselines from 21 to  $73\lambda$ .



In figure 7, a core array using 37 hexagonal modules in a hexagonal grid of 7 lines is shown, in the same format as figure 6. In such an array, a total of 63 baselines can be observed. Using 10 modules, one configuration which achieves 44 baselines (one baseline occurring twice) has been found, which is indicated by the shaded modules in the left part of the figure. The baseline coverage is shown in the right part of the figure, with the twice-covered baseline shaded. The modules and baselines to be used for real-time monitoring are marked with an “R” as before. Reducing to 9 modules, there is a symmetric pattern which produces 36 nonredundant baselines, while increasing to 11 modules gives a maximum of 49 baselines.

For a total array diameter of about 80 m, each module should comprise 91 elements in 11 rows, for a total of 3367 elements. 27-row modules gives a diameter of 183 m and 20239 elements total. The baselines for 17-row modules are from 13.25 to 69  $\lambda$ , while 27-row modules give baselines from 21 to 109  $\lambda$ .

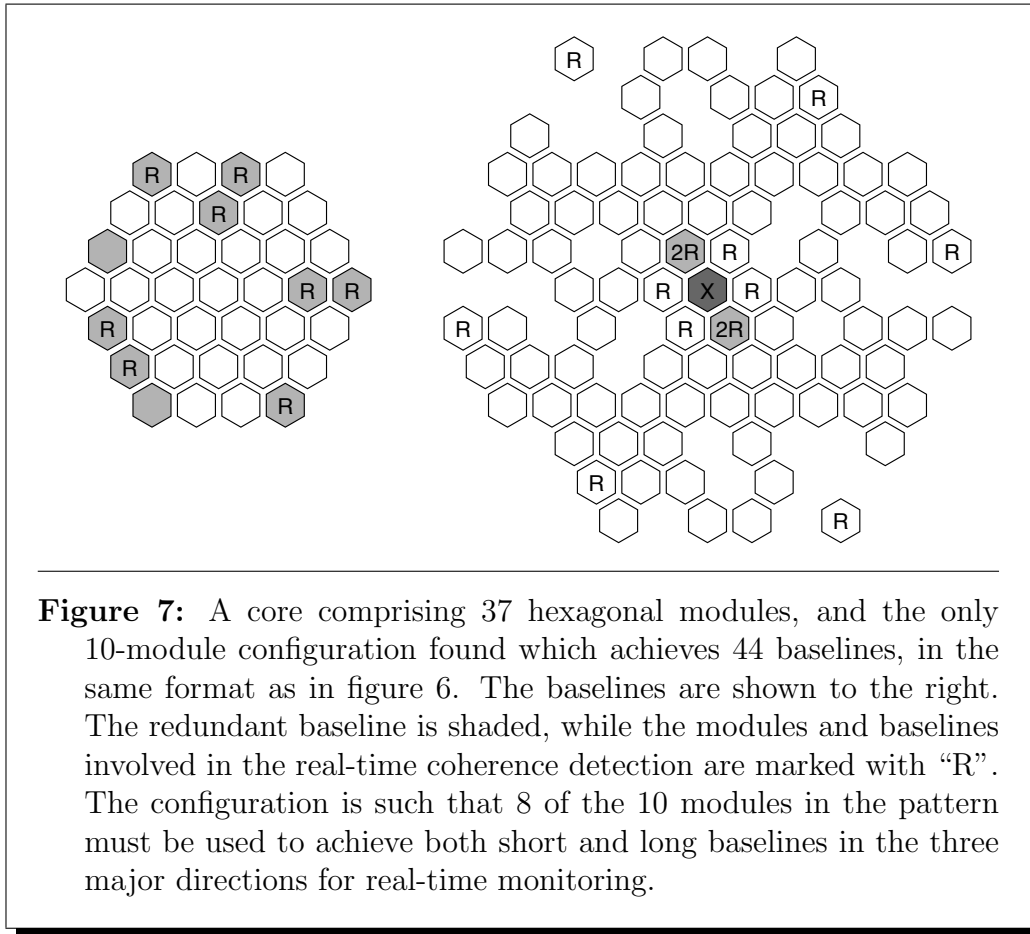


**Figure 7:** A core comprising 37 hexagonal modules, and the only 10-module configuration found which achieves 44 baselines, in the same format as in figure 6. The baselines are shown to the right. The redundant baseline is shaded, while the modules and baselines involved in the real-time coherence detection are marked with “R”. The configuration is such that 8 of the 10 modules in the pattern must be used to achieve both short and long baselines in the three major directions for real-time monitoring.

### 3.2 Configuration of outlier modules

With a main array diameter of about 80 m ( $D \approx 64 \lambda$ ) for the first stage, it is not possible to achieve long enough baselines for detailed imaging within the main array. We have assumed that these will be passive, but otherwise identical to the modules in the core.

Since outlier modules will be used primarily for interferometry, their positions are determined solely by how useful they are for imaging. The core will provide all short baselines, but the exact core configuration will not make a great difference in the long baselines. When simulating different outlier configurations, a single core was used, the 8-module configuration shown in figure 4.

The “synthesised beam” is the 2-dimensional Fourier transform of the baseline pattern. Consequently, the starting point for imaging is the convolution of the synthesised beam with the true image. Therefore, this beam should

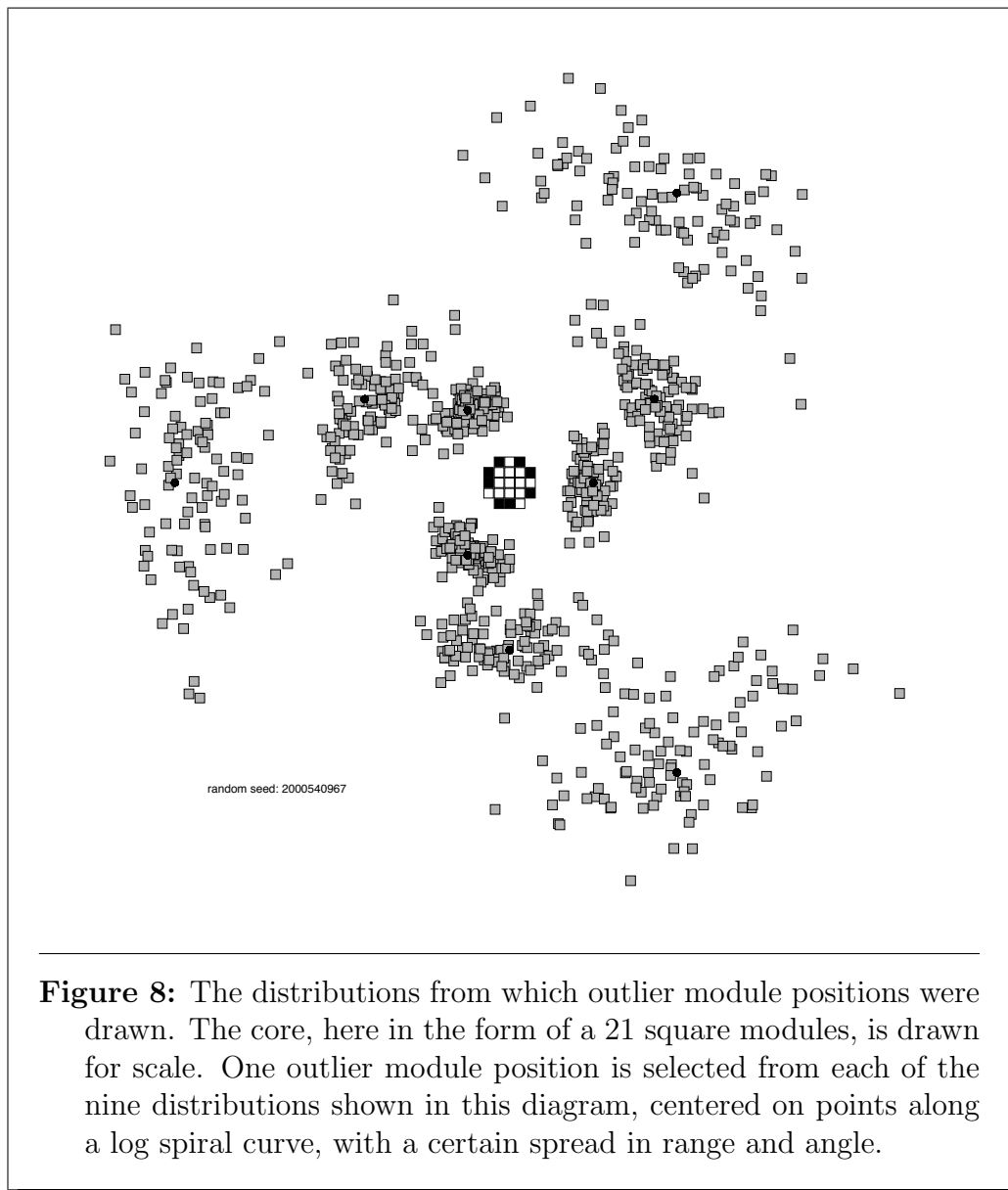
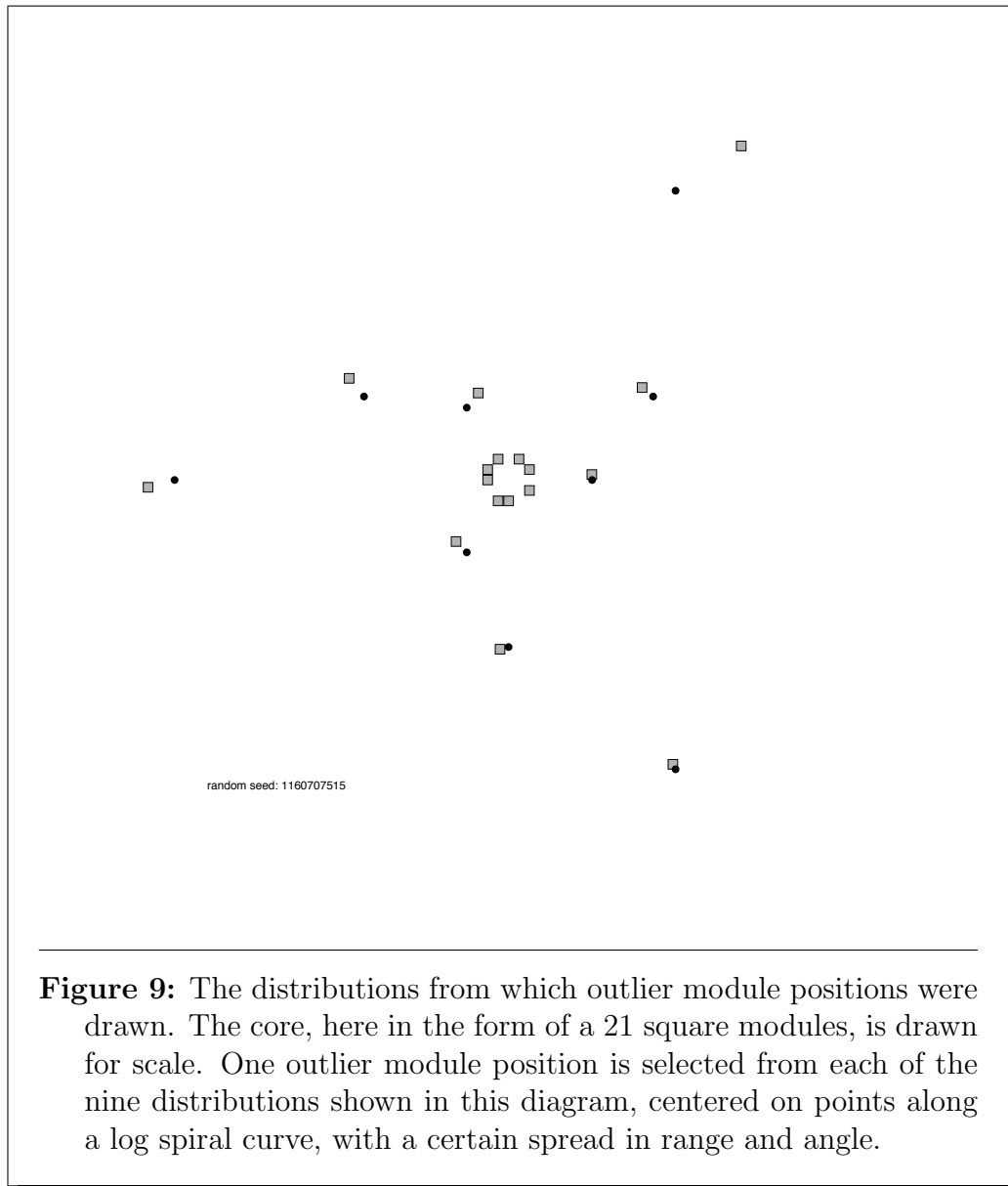


**Figure 8:** The distributions from which outlier module positions were drawn. The core, here in the form of a 21 square modules, is drawn for scale. One outlier module position is selected from each of the nine distributions shown in this diagram, centered on points along a log spiral curve, with a certain spread in range and angle.

be as cleanly defined as possible, to give the image inversion algorithm a good initial estimate. Module configurations were evaluated by the maximum sidelobe level in the synthesised beam inside a region in the vicinity of the on-axis position. Since regularities in the module positions also create regularities in the baseline pattern, which again create excessive sidelobes in the synthesised beam, the module positions are randomised around some nominal positions chosen to provide good coverage on several scales.



Based on experiences from radio astronomy, nominal module positions were sought along log-spiral arms. A total of nine modules were positioned at three different distances on evenly spaced arms. Positions were then chosen at random from distributions centered on these nominal positions, but with a spread in azimuth angle and range. Figure 8 shows 100 positions drawn from each of these distributions, centered on the black dots. The core, in this case, is 108 m in diameter, and the centre points of the distributions are

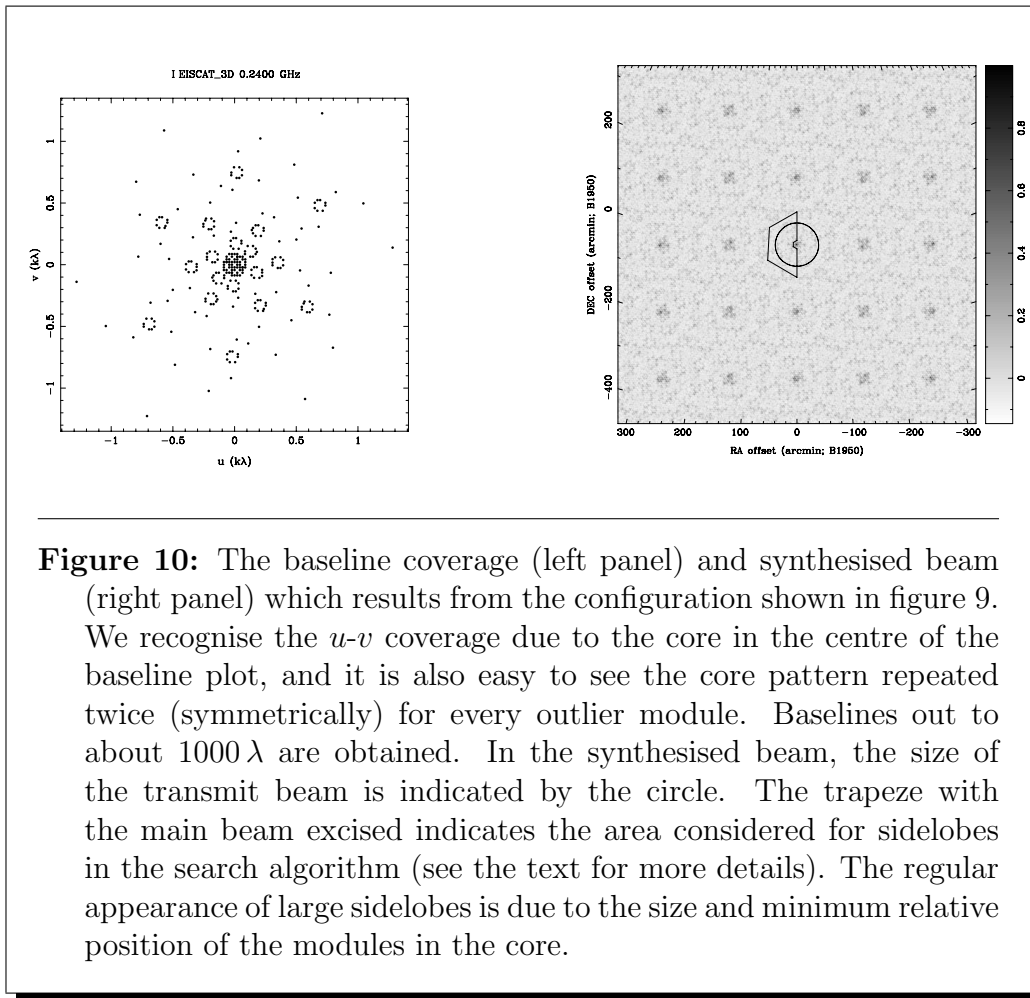


**Figure 10:** The baseline coverage (left panel) and synthesised beam (right panel) which results from the configuration shown in figure 9. We recognise the  $u$ - $v$  coverage due to the core in the centre of the baseline plot, and it is also easy to see the core pattern repeated twice (symmetrically) for every outlier module. Baselines out to about  $1000 \lambda$  are obtained. In the synthesised beam, the size of the transmit beam is indicated by the circle. The trapeze with the main beam excised indicates the area considered for sidelobes in the search algorithm (see the text for more details). The regular appearance of large sidelobes is due to the size and minimum relative position of the modules in the core.

at distances of 108, 216 and 432 m from the centre of the core. For larger cores, the size of the arms is stretched accordingly.

The best configuration found during such a search is shown in figure 9, with module positions shown as grey squares and the distribution centre points are shown as black dots. The  $u$ - $v$  coverage and resulting synthesised beam are shown in figure 10. It is interesting to see how the square modules result in a rectangular pattern of high sidelobes, while the roughly triangular arrangement of the outlier modules results in hexagonal patterns of close-in sidelobes.

## 4 Configurations and site selection

The simulations above are not taking any environmental factors into account. When potential sites are surveyed, it will not always be possible to place outlier modules in every desirable position. On the other hand, there is considerable possibility for finding quite different configuration with equally good statistics in the sidelobes of the synthesised beam.

For site selection purposes, taking a pattern like that in figure 9 and trying to find a site where it can be placed, might result in sites which are less than optimal for a number of reasons. Instead, we suggest to create a template which includes a core area of diameter and shape as decided upon in this design process, and then add diffuse “outlier zones” corresponding to the distributions used when creating figure 8. Site selection can then be made such that there are as few obstacles as possible within these outlier zones. After site selection is finished, another search can be made, this time with actual obstacles included in the search program, and the best possible configuration can be found for the particular site.

### 4.1 What baselines to monitor for real-time decision

A given baseline implies an upper limit to the structure size that can be observed. For instance, the 132 m baseline of the ESR ( $D = 220 \lambda$ ) implies a practical angular size limit of about 0.001 radians (500 m at 500 km range). The relation between structure size, baseline (or its inverse, fringe size) and coherence is given by figure 2 of [1], reproduced as figure 1 of [3]. We see that the smallest scattering structures will produce high coherence almost regardless of baseline, while larger structures will only produce high coherence in shorter baselines. The choice of which baselines to monitor for real-time decision is therefore also a choice of what kinds of events to look for. If only the narrowest of structures are considered to be of interest, the longest baselines can be used for the decision-making. To catch as many events as possible, shorter baselines should be used as well.

- recommend initially to monitor two short ( $\sim 15 \lambda$ ) and two intermediate ( $\sim 50 \lambda$ ) baselines at angles to each other, e.g. two N-S and two E-W

### acknowledgment

Great thanks are due to D. J. McKay for fruitful discussions and insights in radio astronomy principles and practices, and for assistance in setting up the simulations.

## References

- [1] T. Grydeland, E. M. Blixt, U. P. Løvhaug, T. Hagfors, C La Hoz, and T. S. Trondsen. Interferometric radar observations of filamented structures due to plasma instabilities and their relation to dynamic auroral rays. *Ann. Geophys.*, 22(4):1115–1132, 2004.
- [2] Peter H. Hildebrand and R. S. Sekhon. Objective determination of the noise level in Doppler spectra. *J. Appl. Meteor.*, 13(7):808–811, 1974.
- [3] César La Hoz and Tom Grydeland. Considerations and requirements regarding WP5: Interferometry. report for the EISCAT\_3D project, 10. Sep 2005.
- [4] D. J. McKay. EISCAT-3D WP4/5/8/9 signal processing meeting. summary of discussions from the meeting at 2006-07-03, 05. Jul 2006.
- [5] D. J. McKay. EISCAT-3D WP5 discussion document #1. summary of discussions before the meeting at 2006-07-03, 27. Jun 2006.